Chemical Engineering Journal 97 (2004) 257–263

Chemical Engineering Journal

www.elsevier.com/locate/cej

Shear stress-based modelling of steady state permeate flux in microfiltration enhanced by two-phase flows

P. Pospíšil [a], R.J. Wakeman [b], I.O.A. Hodgson [b], P. Mikulášek [a,*]

[a] *Department of Chemical Engineering, Faculty of Chemical Technology, University of Pardubice, nám. Čs. Legií 565, Pardubice 532 10, Czech Republic*
[b] *Department of Chemical Engineering, Loughborough University, Loughborough LE11 3TU, UK*

Accepted 26 May 2003

Abstract

Crossflow microfiltration experiments without intensification and with two-phase gas–liquid flow were performed on aqueous titanium dioxide dispersions using an alumina tubular membrane. The influence of gas flow velocity on flux was studied. The empirical model for steady state permeate flux and cake thickness prediction was developed. The results of experiments show positive effects of constant gas–liquid two-phase flow on the flux. It was found that there are no operating conditions at which air injection has no effect on the permeate flux. From analysis of the experimental results without gas flow, the empirical model based on Darcy's Law and on mass balance over a membrane module was derived. The model is based on dimensionless numbers regression of all basic operating conditions that influence permeate flux and cake thickness. The results showed good agreement between model prediction and experimental data with gas injection tested on the same apparatus. When the data from a different system (membrane type, membrane material) were taken, the agreement was not so good.

Keywords: Microfiltration; Modelling; Wall shear stress; Gas–liquid two-phase flow

1. Introduction

Crossflow microfiltration is a pressure driven membrane process for separating dispersed matters in range of sizes from 0.05 to 10 μm from liquids. The principle of solid/liquid separation can be described as a pressing of pure liquid through the membrane pores and through the deposit of solid particles on the membrane wall. In the absence of membrane fouling, the increasing thickness of the deposit of particles (cake formation) causes the initial rapid decrease of flux, and limits the wider application of microfiltration. In spite of this, the separation process finds increasing use in water purification, wastewater treatment, brewing and biotechnology industries, amongst others.

The key goals in the design of crossflow microfiltration are preventing cake formation and thereby increasing the permeate flux. The prediction of steady state permeate flux, as a function of the operating conditions, would be a very useful aid to the design procedure. A wide range of flux enhancement methods have been developed and experimentally tested in recent years. Surveys of these methods are summarised in the literature [1,2]. Generally, there are three possible approaches to reduce or control concentration polarization, cake formation and fouling:

1. Changes in surface characteristics of the membrane,
2. Pre-treatment of the feed and
3. Fluid management methods.

In this paper, our attention has been aimed experimentally to one of the fluid management methods and theoretically to the general shear stress-based mathematical model, which in principle, could be used for the prediction of steady state permeate flux for most of fluid management methods.

Use of a gas–liquid two-phase flow technique in the feed stream has been tried during microfiltration and ultrafiltration processes in order to enhance the flux for different applications (biological treatment, drinking water production, macromolecules separation) and different membrane geometry (hollow fibre, flat sheet or tubular). The results of experiments showed in all cases improvement of permeate flux and pointed towards some mechanisms acting near the membrane wall. The description of the impact of gas–liquid two-phase flow on events near the membrane wall is based on a change of hydrodynamic conditions inside the membrane module which positively increases the wall shear stress, preventing membrane fouling and cake formation.

* Corresponding author. Tel.: +420-466037130; fax: +420-466037068.
E-mail address: Petr.Mikulasek@upce.cz (P. Mikulášek).

1385-8947/$ – see front matter
doi:10.1016/j.cej.2003.05.001

Cui and co-workers [3–5] have shown that injecting air can reduce concentration polarization in ultrafiltration of macromolecules (dextran, dyed dextran and bovine serum albumin) in the case of flat sheet modules and hollow fibre membranes. The explanation given for the flux enhancement is that air sparging into the liquid stream increases turbulence near the membrane surface as well as the cross-flow velocity, thus limiting the boundary layer thickness. They also carried out airlift cross-flow ultrafiltration experiments and reached flux increasing of up to 320%.

Mercier et al. [6,7] obtained significant flux enhancement (200% increase of flux) by air sparging in ultrafiltration tubular inorganic membranes with bentonite and yeast suspensions. They found that the most advantageous flow regime for intensification is plug flow. Membrane position during air sparged ultrafiltration and energetic costs have been studied also [8]. Better performance of the ultrafiltration process with gas sparging has been imputed to higher wall shear stress, local variations of pressure in the membrane module and to increased turbulence and local mixing [9].

Cabassud and co-workers [10–12] have presented results concerning two-phase gas–liquid flow for particle suspensions (clay suspensions) inside hollow fibres. In that case, flux improvement was linked to hydrodynamic control of the particle deposition on the membrane. Significant increases in permeate flux have been observed, even at a very low air velocity, for all the concentrations studied. The air injection process leads to an increase of up to 155% at specific conditions. However, good results have been obtained for very low air velocities (under $0.2\,\mathrm{m\,s^{-1}}$). It was also shown that the presence of gas in the membrane module decreased pore blocking (fouling), with partial flushing out of the deposited cake. Increased cake thickness with increasing gas flow velocity caused a higher cake porosity, which also led to an improved permeate flux [10,11].

Lee et al. [13] used air slugs entrapped in the cross-flow stream to prevent the flux decline during filtration of bacterial cell suspensions. Ultrafiltration and microfiltration flat sheet membranes were used and the best performance was obtained for the ultrafiltration (a maximum enhancement of 200% was reported). Unlike Cabassud et al. [10–12], it was reported that the gas sparging had insignificant influence on membrane pore fouling.

The removal of cake deposition from the outer surface of hollow fibre membranes immersed in a wastewater treatment bioreactor has been studied by Bouhabila et al. [14]. They found that the intensification impact of air was effective until the airflow velocity reached a critical value. From the point of view of purified water quality, the presence of gas shortened the residence time of the liquid in bioreactor, leading to a worsening of the water quality.

Chang et al. [15,16] studied the influence of the hollow fibre membrane module on process efficiency; they showed that a vertical orientation is better than a horizontal one. Otherwise they found that gas sparging can remove or weaken newly deposited filter cake, but cannot remove cake deposited on the membrane wall before gas sparging was started.

Noriatsu et al. [17] validated better elimination of cake deposits with increasing wall shear stress; their experiments were carried out with the flat sheet membranes filtering wastewaters. Mi-Jung et al. [18] performed ultrafiltration of oil wastewaters and found problems with pore blocking by gas bubbles when the bubbly regime of a gas–liquid flow was used.

An accurate model that enables prediction of permeate flux during microfiltration with two-phase flow has not yet been proposed. Vera et al. [19] expressed steady state flux of gas-sparged microfiltration and ultrafiltration using two dimensionless numbers: a generalised shear stress number and a resistance number. Their experiments were carried out with dextran, wastewater effluent, tap water and ferric hydroxide suspensions and they achieved maximum flux enhancement of 200%.

The ultrafiltration model of Ghosh et al. [20] is based on a diffusion transport mechanism of permeate through the membrane surface and gives values of predicted flux lower then experimental ones. The model consisted of dividing the two-phase flow in the membrane into three zones enclosed in one gas slug.

In this paper, the gas–liquid two-phase flow intensification method used for microfiltration of titanium dioxide dispersions on tubular ceramic membrane is presented. The goal of this paper is the wall shear stress-based calculation of the steady state permeate flux, developed from Darcy's Law adapted for our experimental system and from a mass balance solved by Datta et al. [21]. The validation of this model by laboratory experiments is also presented.

2. Theoretical development

Calculation of permeate flux from Darcy's Law is based on the knowledge of hydraulic resistance and the thickness of the filter cake, and on a knowledge of the membrane resistance. In the filter system, which allows penetration of particles into the membrane pores or surface pore blocking, the pore blocking resistance has to be included also. In that case

$$J_{SS} = \frac{\Delta P}{\mu_0 (R_M + R_{BL} + r\delta)} \tag{1}$$

where J_{SS} is the steady state permeate flux, ΔP is the transmembrane pressure difference, μ_0 is the solvent viscosity, δ is the cake thickness, R_M, R_{BL} and r are the membrane, blocking and hydraulic cake resistances, respectively. The membrane resistance can be determined from the pure water filtration experiment and is expressed as $R_M = \Delta P/\mu_0 J_0$. The hydraulic cake resistance is estimated using the Blake–Kozeny correlation

$$r = \frac{45\phi_{max}^2}{a^2(1-\phi_{max})^3} \tag{2}$$

where ϕ_{max} is the maximum volume fraction of particles packed in the cake and a is the particle radius.

The result of microscopic mass balances for particles and the dispersing liquid along the creeping filter cake [21] was used by Mikulasek et al. [22]. The steady state thickness of the cake results in the value of steady state permeate flux and is limited by operating conditions of the microfiltration process. This dynamic balance maintains the steady state flux and is controlled by the shear stress on the surface of the cake, which is a function of the initial shear stress on the clean membrane surface, τ. The steady state flux is expressed as [21]

$$J_{SS} = \frac{(\phi_{max} - \phi_B)}{\phi_B} \frac{\tau}{\mu_C} \frac{\delta^2}{2L} \quad (3)$$

where ϕ_B is the volume fraction of particles in the feed, μ_C is the cake apparent viscosity (calculated from the Mooney equation, $\mu_C = \mu_0 \exp(2.5 \times \phi_{max} \times 0.74/(0.74–\phi_{max}))$) and L is the membrane length. This equation was validated experimentally [21,22] and gave good agreement between the theoretical and experimental results. Hence, we have chosen it to create dimensionless model to predict steady state permeate flux in enhanced microfiltration.

Darcy's law, Eq. (1), compares the process driving force and the resistance to permeate flow. When there is no resistance to fluid flow offered by the membrane or by pore blocking, the permeate flux is inversely proportional to the cake thickness. However, Darcy's equation does not offer any detailed explanation of the relationship between cake thickness and permeate flux when pore blocking occurs. Eq. (3) relates the permeate flux to the wall shear stress (that is, the shear stress at the membrane surface), and shows that flux is proportional to the cake thickness. The ratio of the wall shear stress to the applied pressure difference is then inversely proportional to δ^3, which is entirely consistent with equations developed previously [23] but using a different model for the wall shear stress. Furthermore, according to Eq. (3) the longer is membrane the higher is the resistance to permeate flow, while the cake thickness is constant from some location measured from the feed side of membrane.

The dimensionless quantities $N_1 = R_{BL}/R_M$, $N_2 = \tau/\Delta P$ and $N_3 = \delta/d$, $N_4 = \Delta P/\rho u^2$ have been deduced semi-empirically from data measured during microfiltration without intensification and plotted for various concentrations. The relations between numbers N_1 and N_2, and between N_3 and N_4, respectively, give us a general overview of the mutual influences of the operating conditions on permeate flux and cake thickness. Two mathematical equations have been found from interpretation of the experimental data, and they relate the dimensionless numbers to feed concentrations expressed as volume fraction of solid particles in liquid. When the operating conditions of microfiltration process are known, as well as the parameters of membrane and feed dispersion, we can predict cake thickness and pore blocking resistance and consecutively permeate flux from Eq. (1). The equations for prediction of R_{BL} and δ are represented by the relationships

$$\frac{R_{BL}}{R_M} = (0.0009\phi^{0.4961}) \left(\frac{\tau}{\Delta P}\right)^{-0.875} \quad (4)$$

and

$$\frac{\delta}{d} = (0.0149\phi^{0.5136}) \left(\frac{\Delta P}{\rho u^2}\right)^{(0.0146\phi^{-0.4498})} \quad (5)$$

where d is the membrane diameter (or hydraulic diameter of the feed channel cross-section when the membrane is not tubular), ρ is the feed density and u is the feed flow velocity. Eqs. (4) and (5) were obtained using a feed concentration in the range from 1 to 5% (v/v), a transmembrane pressure difference in the range 50–200 kPa, and a feed flow velocity in the range 0.5–4 m s^{-1}.

3. Experimental

The experimental apparatus is shown schematically in Fig. 1. A variable speed pump was used to feed a dispersion to the membrane module from the temperature controlled storage tank. The pressure difference was controlled by a control valve placed downstream of the membrane module. The feed and gas flow velocities were measured by flow meters and maintained constant. All the operating conditions (transmembrane pressure, feed and gas flow velocities, gas flow mode) have been monitored by computer, which also logged data relating to the mass of permeate collected, from which it calculated the value of permeate flux. Gas was sparged into the feed stream just before it entered the membrane module during the enhanced experiments. Feed flow velocities of 0.5–4 m s^{-1}, gas flow velocities of 0.2–3 m s^{-1} and transmembrane pressures of 50–200 kPa were studied. By systematically adjusting one parameter while maintaining the others constant, steady state permeate flux values were obtained as a function of each variable. All the experiments were conducted at a temperature of 25 ± 2 °C.

The suspension studied comprised of TiO_2 (rutile) suspended at a known concentration (volume of particles/volume of liquid) in distilled water. The concentrated suspension was supplied by Ostacolor a.s, Pardubice, Czech Republic and then diluted. The mean particle diameter was measured by Light Scattering machine (ZetaPals, BIC, USA) and was equal to 400 nm, but the size distribution was very wide. The pH of the dispersions was not adjusted and its value was close to 8.0.

The ceramic membranes used in this work were asymmetric, three-layered, made of alumina (produced by Terronic, Hradec Kralove, Czech Republic). They were configured as single cylindrical tubes 0.45 m long with inner diameter 6 mm and with the active surface on the inner side. The pore size distribution measured by the modified bubble test was narrow and mean pore diameter was equal to 91 nm. After every filtration, the membranes were cleaned in an

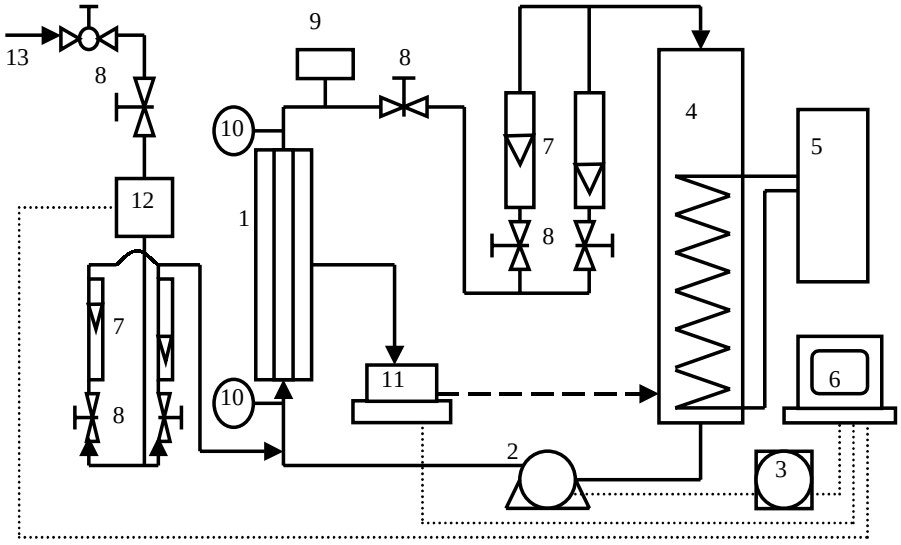

Fig. 1. Set up of experimental apparatus (1) microfiltration module, (2) pump, (3) pump regulator, (4) storage tank, (5) thermal regulating system, (6) computer, (7) flowmeters, (8) valves, (9) pressure indicator, (10) pressure gauge, (11) electronic balance, (12) solenoid valve, (13) air inlet.

ultrasonic cell and stored in dry place. They were wetted overnight before next usage.

4. Results and discussion

Membrane pure water flux and membrane resistance values were characterised by distilled water microfiltration experiments. The ceramic membrane resistance was taken as a reciprocal value of the slope of plotted pure water flux against the transmembrane pressure divided by water viscosity, from which the value of $3.33 \times 10^{12}\,\mathrm{m}^{-1}$ was obtained. The hydraulic cake resistance of rutile calculated using the Blake–Kozeny correlation was $1.11 \times 10^{16}\,\mathrm{m}^{-2}$ (the maximum volume fraction of particles packed in the cake is equal to 0.65 [22]). Analysis of the permeate showed complete retention of the rutile in the feed.

Experiments without gas–liquid two-phase flow confirmed the known behaviour of the flux with time. The initial decrease of flux was quite linear and rapid and the steady state flux was reached after 1–2 h—this was a value about five times lower than the initial flux. Obviously, the steady state value could have been increased, and was done so experimentally by increasing the feed flow velocity (with parallel lowering of the feed concentration or pressure difference—but this way is more energetically and investment demanding). So, there is a room for intensification methods in this process development—we tested one of them, gas–liquid two-phase flow of the feed stream inside the tubular ceramic membrane.

Direct observations through the transparent tubular pipe of the same ID as the membranes showed that our experiments with gas–liquid two-phase flow gave rise to the following flow patterns:

1. bubble flow—about 25% of experiments, in the region of low gas and liquid flow velocities;
2. slug flow—about 50% of experiments, in the region of medium gas and liquid flow velocities and
3. churn flow—about 25% of experiments, in the region of the highest gas and liquid flow velocities.

Generally, the bubble flow pattern was achieved at low gas and liquid flow velocities ($0.2 < u_G \leq 0.5\,\mathrm{m\,s}^{-1}$, $0.5 < u \leq 0.75\,\mathrm{m\,s}^{-1}$), slug flow was observed with intermediate conditions ($0.5 < u_G \leq 1.5\,\mathrm{m\,s}^{-1}$, $0.75 < u \leq 1.75\,\mathrm{m\,s}^{-1}$) and churn flow occurred at higher flow rates ($u_G > 1.5\,\mathrm{m\,s}^{-1}$, $u > 1.75\,\mathrm{m\,s}^{-1}$).

Previous work showed that slug flow is the most efficient regime for significant enhancement of mass transfer [6,10]. It should be noted that for a given liquid flow rate, the presence of the gas increases the mean longitudinal velocity of the fluid, and in association with the great variations in the wall shear stress and the turbulence, can improve the process performance. The effects of gas–liquid two-phase flow on permeate flux were measured for various experimental conditions and the permeate flux obtained was always larger than that without gas flow. Nevertheless, behaviour of the flux-time curves showed similar forms to those without gas flow, but the flux decline was neither so rapid nor so extreme. The permeate flux has been maintained at a higher level during the filtering period.

The values of the normalised steady state permeate flux are plotted as a function of superficial gas flow velocity in Figs. 2 and 3 for feed concentrations of 1 and 5% (v/v), respectively. Differences between the results of experiments carried out with the transmembrane pressure difference of 100 and 200 kPa can be observed on Fig. 2. When the pressure of 100 kPa was applied, the increase of steady state flux compared to the same filter conditions without gas flow was

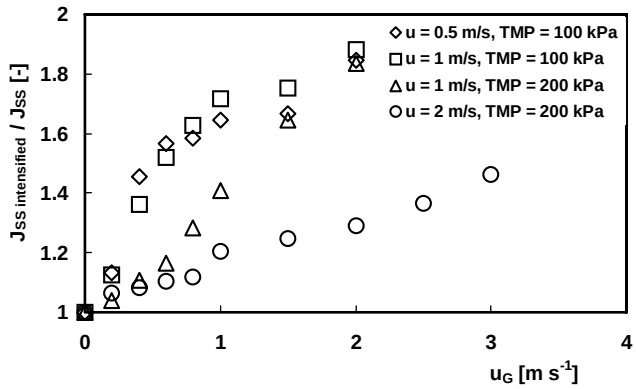

Fig. 2. Normalised steady state permeate flux as function of the gas flow velocity for various liquid flow velocities and transmembrane pressures; feed concentration $\phi_B = 0.01$.

quiet sharp even at low gas flow velocities (increase of 50% for $u_G = 0.5\,m\,s^{-1}$). From Fig. 2, the form of the curves is independent of the superficial liquid flow velocity, and it is interesting that the plateau occurs in the regime of slug flow for gas flow velocities from 0.8–1.5 $m\,s^{-1}$. When the pressure of 200 kPa was applied, the increase of steady state flux was not so sharp, and above $u_G = 0.5\,m\,s^{-1}$ the form of the curve shows differences for various liquid flow velocities. The intensification outcome during the experiments with dispersion of 5% (v/v) shows that the impact of gas flow was similar for all conditions applied (Fig. 3). Generally, the enhancement of permeate flux was the most effective when the operating conditions allowing formation of the thicker cake occurred (low feed flow velocity, high pressure).

Study of the effect of the dispersion concentration on permeate flux was undertaken by comparing the conventional single-phase cross-flow microfiltration with two-phase flow membrane system. It is interesting to note that the concentration reached with two-phase gas–liquid flow was twice as high as the concentration reached without intensification for the same filtration time. This fact can be advantageous

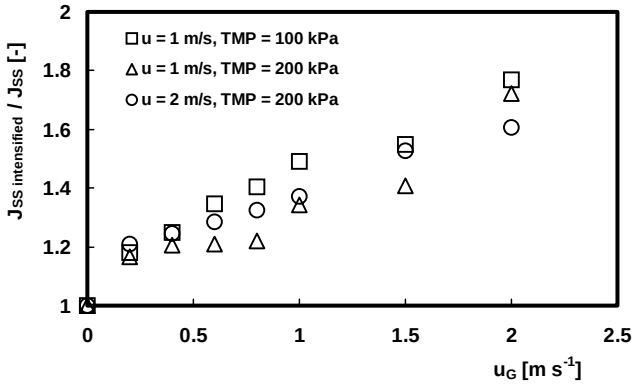

Fig. 3. Normalised steady state permeate flux as function of the gas flow velocity for various liquid flow velocities and transmembrane pressures; feed concentration $\phi_B = 0.05$.

in processes where rapid concentration of a dispersion is required. The most important consideration is that for all the concentrations in the range tested, an enhancement of the permeate flux is always observed because of the air injection. There is no concentration for which air injection has no effect on the flux.

5. Model validation

The model was validated using the sets of data from microfiltration of rutile with two-phase flow, using the same microfiltration apparatus as for measurements of rutile without two-phase flow.

Although the value of membrane resistance was high in the case of our experimental set up, the resistance of the cake deposit limited the magnitude of the steady state permeate flux reached. The hydraulic resistance of the cake is constant when calculated from the Blake–Kozeny correlation and its value changes only with the state of the dispersion, the maximum volume fraction of particles packed in the cake and with the particle radius. So the overall cake resistance depended only on the cake thickness; we assumed an incompressible cake of constant porosity. When an appropriate ratio of particle size and pore diameter are chosen for the experimentation, the influence of the pore blocking resistance would be negligible. But in our system, the particle size distribution was very wide and pore blocking had to be taken into account.

Fig. 4 shows the change of cake thickness with wall shear stress for various filtration conditions used during the experiments with gas flow. Cake thickness values were calculated from Eq. (5). It can be seen that the significant effect on cake thickness was predominantly caused by concentration of the feed, but it is interesting that for any one concentration, the change of cake thickness with increasing shear stress was of secondary importance. The difference between results for various pressures can be observed. This may indicate that the value of wall shear stress calculated for clean membrane is not that one which really impacts on the growing cake,

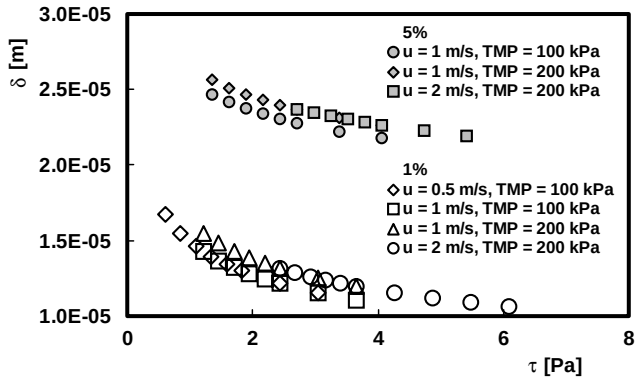

Fig. 4. Influence of wall shear stress on cake thickness for various operating conditions.

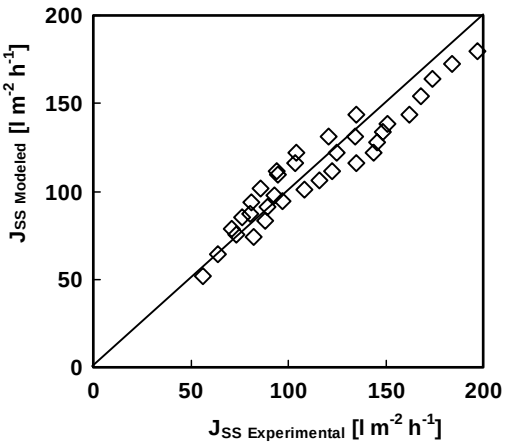

Fig. 5. Comparison of experimentally measured and calculated permeate fluxes for feed concentration $\phi_B = 0.01$.

because the shear stress during the cross-flow microfiltration decreases to zero on the membrane wall with increasing cake thickness, and increases on the edge of the growing cake because of lowering cross-section for feed flow [23].

Figs. 5 and 6 show the values of steady state permeate flux experimentally measured and predicted by the model. Fig. 5 compares values for rutile suspensions with a concentration of 1% (v/v) filtered with two-phase gas–liquid flow, Fig. 6 compares values for rutile suspensions with a concentration of 5% (v/v) filtered with two-phase gas–liquid flow.

The experimental conditions under which the permeate fluxes shown in Figs. 5 and 6 were measured and calculated are:

- transmembrane pressure differences: 50, 100 and 200 kPa,
- feed flow velocities: 0.5, 1, 1.5, 2, 3 and 4 m s^{-1},
- gas flow velocities: 0.2, 0.4, 0.6, 0.8, 1, 1.5, 2 and 3 m s^{-1}.

The quantitative agreement between theory and experiments is good in the case of rutile, especially for a feed concentration 1% (v/v). For the experimental data measured on the different systems the model tends to overpredict steady state permeate flux. This may be caused by the high permeability of the synthetic membranes (relatively low membrane resistance compared to ceramic membranes) and by the different membrane configuration (flat sheet rather than tubular). Worse agreement of the model with the experimental data in Fig. 6 is thought to have occurred due to slight foaming of the feed during the experiments, with the feed concentrated of 5% (v/v). It caused unstable flow conditions and therefore resulting fluxes.

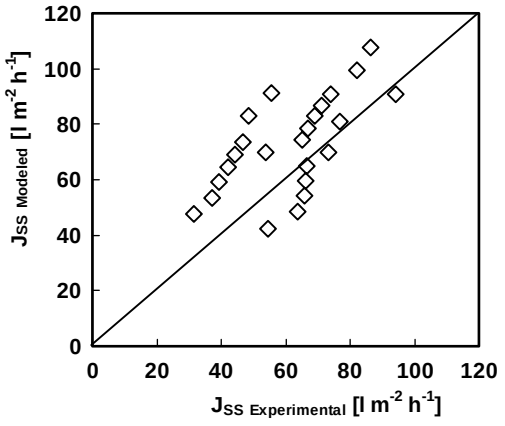

Fig. 6. Comparison of experimentally measured and calculated permeate fluxes for feed concentration $\phi_B = 0.05$.

6. Conclusions

The effect of superficial gas flow velocity on the steady state permeate flux improvement has been presented for various operating conditions used. The results show an increased flux in all experiments for aqueous dispersions of titanium dioxide (rutile) that were crossflow microfiltered in a ceramic tubular membrane. A maximum flux improvement of 90% was achieved when the operating conditions with gas flow of $u_G = 2.0\,m\,s^{-1}$, a superficial feed velocity of $u = 1.0\,m\,s^{-1}$ and $\Delta P = 100\,kPa$.

A mathematical model of steady state cake thickness and permeate flux based on Darcy's Law and the mass balance in membrane module has been presented. Empirical equations derived from microfiltration experiments without gas flow suitable for the systems where the pore blocking occurs were regressed. The validation of the model was tested on the data with two-phase gas–liquid flow with good agreement. The difference between experimental and model results varied from:

- +19% to −15% for rutile of 1% (v/v), with gas enhancement,
- +70% to −24% for rutile of 5% (v/v), with gas enhancement.

List of symbols

a	particle radius (m)
d	membrane tube inner diameter (m)
J_{SS}	steady state permeate flux (m s^{-1}) (l m^{-2} h^{-1})
J_0	pure water permeate flux (m s^{-1}) (l m^{-2} h^{-1})
L	membrane length (m)
ΔP	transmembrane pressure difference (Pa)
r	hydraulic cake resistance (m^{-2})
R_M	membrane resistance (m^{-1})
R_{BL}	pore blocking resistance (m^{-1})
t	time (s)
u	superficial liquid flow velocity (m s^{-1})
u_G	superficial gas flow velocity (m s^{-1})
δ	cake thickness (m)
μ_0	permeate viscosity (Pa s)
μ_C	apparent viscosity (Pa s)
ϕ_{max}	maximum volume fraction of particles packed in the cake (−)

ϕ_B volume fraction of particles in the feed (-)
ρ feed density (kg m^{-3})
τ wall shear stress (Pa)

Acknowledgements

P. Pospíšil is grateful to Socrates/Erasmus European Union exchange programme for the financial aid, and to University Pardubice for the International Cooperation Development Grant, which enabled his study stay at Loughborough University.

References

[1] P. Mikulášek, Collect. Czech. Chem. Commun. 59 (1994) 737.
[2] R. Wakeman, C. Williams, Memb. Tech. 124 (2000) 4.
[3] Z.F. Cui, K.I.T. Wright, J. Memb. Sci. 117 (1996) 109.
[4] Z.F. Cui, S.R. Bellara, P. Homewood, J. Memb. Sci. 128 (1997) 83.
[5] Q.Y. Li, Z.F. Cui, D.S. Pepper, Chem. Eng. J. 67 (1997) 71.
[6] M. Mercier, C. Fonade, C. Lafforgue-Delorme, Biotech. Tech. 12 (1995) 853.
[7] M. Mercier, C. Fonade, C. Lafforgue-Delorme, J. Memb. Sci. 128 (1997) 103.
[8] M. Mercier-Bonin, C. Lagane, J. Memb. Sci. 180 (2000) 93.
[9] M. Mercier-Bonin, C. Maranges, C. Lafforgue, C. Fonade, AIChE J. 46 (2000) 476.
[10] C. Cabassud, S. Laborie, J.M. Lainé, J. Memb. Sci. 128 (1997) 93.
[11] S. Laborie, C. Cabassud, L. Durand-Bourlier, J.M. Lainé, Filtr. Sep. 34 (1997) 887.
[12] C. Cabassud, S. Laborie, L. Durand-Bourlier, J.M. Lainé, J. Memb. Sci. 181 (2001) 57.
[13] Ch.K. Lee, W.G. Chang, Y.H. Ju, Biotech. Bioeng. 41 (1993) 525.
[14] E.H. Bouhabila, R.B. Aim, H. Buisson, Desalination 118 (1998) 315.
[15] S. Chang, A.G. Fane, J. Memb. Sci. 180 (2000) 57.
[16] S. Chang, A.G. Fane, J. Chem. Tech. Biotech. 75 (2000) 533.
[17] O. Noriatsu, Y. Kazuo, Water Res. 35 (2001) 3137.
[18] U. Mi-Jung, Y. Seong-Hoon, L. Chung-Hak, C. Kun-Yong, K. Jae-Jin, Water Res. 35 (2001) 4095.
[19] L. Vera, S. Delgado, S. Elmaleh, Chem. Eng. Sci. 55 (2000) 3419.
[20] R. Ghosh, Z.F. Cui, J. Memb. Sci. 162 (1999) 91.
[21] S. Datta, J.L. Gaddis, Sep. Sci. Tech. 32 (1997) 327.
[22] P. Mikulášek, R.J. Wakeman, J.Q. Marchant, Chem. Eng. J. 69 (1998) 53.
[23] R.J. Wakeman, Trans. IChemE. 72 (1994) 530.